

Pulsed X-ray Emission from The Fastest Millisecond Pulsar PSR B1937+21 with ASCA

Motoki Takahashi^{1,8}, Shinpei Shibata¹, Ken'ichi Torii², Yoshitaka Saito³, Nobuyuki Kawai^{4,2},
Masaharu Hirayama⁵, Tadayasu Dotani³, Shuichi Gunji¹, Hirohisa Sakurai¹, Ingrid H. Stairs^{6,9},
and Richard N. Manchester⁷

ABSTRACT

We have detected pulsed X-ray emission from the fastest millisecond pulsar known, PSR B1937+21 ($P = 1.558$ msec), with ASCA. The pulsar is detected as a point source above ~ 1.7 keV, with no indication of nebulosity. The source flux in the 2–10 keV band is found to be $f = (3.7 \pm 0.6) \times 10^{-13}$ erg s⁻¹ cm⁻², which implies an isotropic luminosity of $L_x = 4\pi D^2 f \sim (5.7 \pm 1.0) \times 10^{32} (D/3.6 \text{ kpc})^2$ erg s⁻¹, where D is the distance, and an X-ray efficiency of $\sim 5 \times 10^{-4}$ relative to the spin-down power of the pulsar.

The pulsation is found at the period predicted by the radio ephemeris with a very narrow primary peak, the width of which is about 1/16 phase ($\sim 100 \mu\text{s}$), near the time resolution limit (61 μs) of the observation. The instantaneous flux in the primary peak (1/16 phase interval) is found to be $(4.0 \pm 0.8) \times 10^{-12}$ erg s⁻¹ cm⁻². Although there is an indication for the secondary peak, we consider its statistical significance too low to claim a definite detection.

The narrow pulse profile and the detection in the 2–10 keV band imply that the X-ray emission is caused by the magnetospheric particle acceleration. Comparison of X-ray and radio arrival times of pulses indicates, within the timing errors, that the X-ray pulse is coincident with the radio interpulse.

¹Department of Physics Yamagata University, Kojirakawa, Yamagata 990-8560, Japan; shibata@sci.kj.yamagata-u.ac.jp

²National Space Development Agency of Japan, Tsukuba Space Center, Space Utilization Research Program, 2-1-1 Sengen, Tsukuba, Ibaraki 305-8505, Japan

³The Institute of Space and Astronautical Science (ISAS), Sagami-hara, Kanagawa 229-8510, Japan

⁴The Institute of Physical and Chemical Research (RIKEN), Wako, Saitama 351-01, Japan

⁵Santa Cruz Institute for Particle Physics, University of California, Santa Cruz, CA 95064

⁶University of Manchester, Jodrell Bank Observatory, Macclesfield, Cheshire, SK11 9DL, UK

⁷Australia Telescope National Facility, CSIRO, Radiophysics, P.O. Box 76, Epping, NSW 1710, Australia

⁸present address: Kunori-Gakuen High School, 1-1-72, Monto-machi, Yonezawa, 992-0039, Japan

⁹present address: NRAO, P.O. Box 2, Green Bank, WV 24944

Subject headings: pulsars: general — pulsars: individual (PSR B1937+21)

1. Introduction

There are two proposed emission regions in the pulsar magnetosphere, the polar cap near the surface of the neutron star and the outer gap near the light cylinder. The magnetic field strength of the polar cap is typically 10^{12} G for the *ordinary pulsars*, while it is typically $10^8 - 10^9$ G, three or four orders of magnitude smaller, for the *millisecond pulsars*. The field strength in the outer gaps near the light cylinder is about 10^6 G for very young ordinary pulsars such as the Crab, while it decreases considerably with spin-down because the light cylinder becomes large: for a period of $P = 0.1$ s, the light cylinder field B_L becomes typically 2×10^4 G. For instance, for Vela, $P = 0.089$ s and $B_L = 4.4 \times 10^4$ G. The field strength at the light cylinder of the millisecond pulsars can exceed the value of the Crab pulsar because of small light cylinder radii. Therefore, if high energy emission from the pulsar magnetosphere is affected by the field strength, comparison of the two pulsar populations in high energy radiation will, plausibly, elucidate the emission and acceleration mechanism. In particular, detections of the millisecond pulsars in X-rays with ROSAT, ASCA, RXTE, Beppo SAX and recently Chandra and XMM Newton are expanding our knowledge of the X-ray emission from the millisecond pulsars.

The fastest millisecond pulsar known is PSR B1937+21 (Backer et al. 1982), which was previously observed with the ROSAT HRI, giving an upper limit on the flux (Verbunt et al. 1996). In this paper, we report the detection of narrow pulses from this pulsar for energies above ~ 1.7 keV in a 100 ks ASCA observation. We give the results of the spatial, temporal and spectral analyses. A comparison with other millisecond pulsars is also given.

2. Observation

We observed PSR B1937+21 with ASCA (Tanaka et al. 1994) on 15–17 November 1997 (50767.959722 – 50769.084027 MJD) for a duration of 97,140 s. The Gas Imaging Spectrometer (GIS; Makishima et al. 1996, Ohashi et al. 1996) was operated at the highest time resolution, $61\mu\text{s}$. In this operation mode, the highest time resolution is obtained at the expense of spatial resolution: the GIS field of view consists of 64×64 pixels of $\sim 0'.98 \times 0'.98$ each. The Solid-state Imaging Spectrometer (SIS; Burke et al. 1991, Burke et al. 1994) was operated in 1-CCD FAINT mode. We screened the event data by the standard selection criteria. The effective exposure time is 57.2 ks for the SIS and 60.0 ks for the GIS, including 38,209 s exposure with the highest time resolution.

3. Spatial Analysis

We present the X-ray contour maps in the GIS soft band (0.7–2 keV) and the GIS hard band (2–10 keV) in Figure 1, and contour maps in the SIS soft band (0.5–2 keV) and in the SIS hard band (2–10 keV) in Figure 2. In the hard band images of both the GIS and the SIS, we clearly detect a source spatially coincident with the radio position within an accuracy of $40''$ (90 % confidence taking into account pointing uncertainties; see Gotthelf 1996).

In order to estimate the background count rate, we take the background region as follows. The GIS background region is a circular region with radius of $20'$ centered on the detector center with subtraction of a circular region with radius of $6'$ centered on the pulsar and an elliptical region with a semi-major axis of $7'$ and a semi-minor axis of $4'$ centered on the soft source seen north of the pulsar (Fig. 1; left panels). Similarly, the SIS background region is the whole chip from which we removed a circular region with radius of $3'$ centered on the pulsar and an elliptical region with a semi-major axis of $2'$ and a semi-minor axis of $1'$ centered on the soft source north of the pulsar.

If we define the source region as a circle with radius $3'$ for the GIS and $1.5'$ for the SIS, centered on the radio position, the source significance, which is estimated by the source flux divided by the background fluctuation, is found to be $\sim 15\sigma$ in the GIS hard band (2-10 keV) and $\sim 5\sigma$ in the SIS hard band (2-10 keV). (These radii of the source regions were found to maximize the source significance; see the last part of this section.) On the other hand, we could not detect the source in the soft band images. Using PIMMS¹⁰ we find that the present result is consistent with the ROSAT non-detection in the 0.1–2.4 keV energy range subject to an inferred interstellar absorption which corresponds to a hydrogen column density of $(0.28 - 2.2) \times 10^{21} \text{ cm}^{-2}$ (Verbunt et al. 1996) and to an assumption of a power law spectrum with index of ~ 1 as suggested by the spectral analysis given below.

We compared the spatial distribution of the events with the point spread function, finding that the source is consistent with a point source. For this analysis, the GIS image is not suitable, but we used the SIS image in the 0.7–10 keV band. Considering the pointing instability, we find that a possible spatial extent must be smaller than $10''$.

For the timing and spectral analyses, we optimized the radius of the source region so that the signal-to-noise ratio was maximized: we searched for the radius for which the source flux divided by the background flux was maximized. In the same way, for the timing analysis, the optimized energy window was also obtained for the GIS data for which the highest time resolution is available. As a result, the optimized radius was found to be $3.0'$ for the GIS data and $1.5'$ for the SIS data; the optimized energy window was 1.7–6.5 keV for the timing analysis.

¹⁰<http://heasarc.gsfc.nasa.gov/Tools/w3pimms.html>

4. Timing Analysis

In the previous section we obtained the optimized spatial and energy regions, i.e., a circular region with the radius $3.0'$ and an energy window of 1.7–6.5 keV. Applying these optimized spatial and energy regions, we collected 227 photons (99 for GIS2 and 128 for GIS3). After converting the arrival times on ASCA to those at the solar system barycenter using TIMECONV¹¹ version 1.53, we searched for a periodicity by folding the photon arrival times into 32 bins with trial periods around the radio period expected from the ephemeris given in Table 1. The χ^2 values calculated relative to a flat distribution are plotted against the trial periods to make a periodogram (Fig. 3). We found a peak of $\chi^2 = 212$ (dof = 31) at $P_{\text{ASCA}} = 1.557806498(9)$ ms, which coincides with the predicted $P_{\text{radio}} = 1.55780649848632017$ ms based on the radio ephemerides (Table 1) with an accuracy higher than $\sim 10^{-11}$ s, which is expected from the duration of the X-ray observation. The peak significance corresponds to 11.15σ (chance probability of 7.4×10^{-29}). We also applied the bin free z_n^2 test (Buccheri et al. 1983) using n -harmonics with several n 's and confirmed the result. Figure 3 illustrates the result of the period search.

We subsequently folded the data using the predicted period P_{radio} , finding the sharply peaked profile shown in the upper panel of Figure 4. It is very difficult to estimate the pulse width accurately because the width is close to the GIS time resolution ($61 \mu\text{s}$). By trying various numbers of phase bins, we estimated it to be $1/16$ ($=0.0625$) phase ($\sim 100 \mu\text{s}$). We examined the energy dependence of the pulse profile, comparing profiles for the softer and harder energy bands, 2–5 keV and 5–10 keV. No significant difference was found.

In the X-ray pulse profile (Fig. 4; upper panel), where we used 32 phase bins, the background level is 3.67 counts/bin indicated by the dashed line. The excess above the background level for the ‘on-pulse’ defined by the phase interval $8.5/32 - 10.5/32$ ($0.266 - 0.328$) is 51.66 counts (19σ), and the excess for the ‘off-pulse’ is 1.93 counts/bin, which is considered to be the DC component. Therefore, out of 51.66 counts in ‘on-pulse’ phase interval, 47.80 counts belong to the pulsed radiation, from which we find a pulsed fraction of $\sim 44\%$. One may notice a possible secondary peak at the phase interval $24.5/32 - 30.5/32$ ($0.766-0.953$). The excess counts for this phase interval above the background is 23.98 counts; i.e., $\sim 5 \sigma$ above the background over these 6 bins. If we regard this excess as the pulsed radiation, then the pulsed fraction is calculated to be $\sim 59\%$. Although the presence of a secondary peak is common in high energy emission from pulsars, in the present observation the limited number of photons does not allow us to determine the count rates for both the secondary pulse component and the DC component simultaneously. Therefore, the presence of the secondary pulse is only tentative.

Since the narrow X-ray pulses were tracked through the observation, a previous estimate

¹¹ Earlier versions are not suitable for the fastest pulsars, because leap seconds are ignored in the calculation of the position of the satellite.

See in detail <http://heasarc.gsfc.nasa.gov/docs/asca/newtimeconv.html>

(Saito 1997) of the ASCA clock stability may be improved to $|\delta f|/f \leq 8 \times 10^{-8}$ for the duration of ~ 100 ks.

We have investigated the alignment of the X-ray pulse peak relative to the radio pulse profile. We used 1400 MHz and 600 MHz observations from the 76-m Lovell Telescope at Jodrell Bank Observatory performed between 1997 Sept. 19 and 1997 Nov. 3, and 430 MHz observations from the 300-m Arecibo telescope performed on 1997 Nov. 22. The radio pulse profiles are very similar at all frequencies used, with the same relative phases of the main pulse and interpulse (Kramer et al. 1999). We aligned these radio data to the same fiducial point, then used the standard pulsar timing program TEMPO (<http://pulsar.princeton.edu/tempo>) to obtain a good local value of the dispersion measure and the ephemeris given in Table 1. We subsequently included the X-ray data in the fit, counting the geocentric arrival time of each X-ray photon within the pulse peak as equivalent to a radio pulse arrival time at infinite frequency. We find that the X-ray peak falls $767 \pm 15 \pm 100 \mu\text{s}$ after the peak of the radio profile main pulse. The latter part of the error comes from the systematic error in absolute time calibration to the ASCA onboard clock. The radio profile interpulse occurs approximately $800 \mu\text{s}$ after the main pulse, so it is plausible, within the timing errors, that the X-ray pulse is coincident with the radio interpulse. In Figure 4 the radio profile is aligned with the X-ray profile.

5. Spectral Analysis

Spectral analysis was performed on the GIS data for which the source region yielded ~ 135 photons after background subtraction. We also tried spectral fits for the data restricted to the ‘on-pulse’ phase. Taking advantage of the phase selection, which enabled us to have a better signal-to-noise ratio, we used a larger aperture of radius $6'$ for the source region; the background region was the same as before but only the ‘off-pulse’ data were used. In this fashion we collected ~ 84 photons.

Unfortunately, the statistics were not sufficient for reliable spectral fits. However, for interstellar hydrogen column densities between $N_{\text{H}} = 2.8 \times 10^{20} \text{ cm}^{-2}$ (see the ROSAT HRI observation; Verbunt et al. 1996) and $N_{\text{H}} = 1.4 \times 10^{22} \text{ cm}^{-2}$ (a typical Galactic hydrogen column density in the direction of the source), we could fit the spectra by power law models (typical reduced $\chi_{\text{r}}^2 \sim 0.8$, d.o.f. = 28). The source flux was found to be $(3.7 \pm 0.6) \times 10^{-13} \text{ erg s}^{-1} \text{ cm}^{-2}$ in the 2 – 10 keV band with a photon index¹² of 0.8 ± 0.6 . On-pulse data were also fitted by a power law model and we found an instantaneous pulsed flux of $(4.0 \pm 0.8) \times 10^{-12} \text{ erg s}^{-1} \text{ cm}^{-2}$ in the 2-10 keV band.

The source is detected in the hard band (2–10 keV) and shows a very narrow pulse. These

¹²The photon index α is defined such that the photon flux is given by $K\epsilon^{-\alpha}$, where ϵ is the photon energy and K is the normalization. We used a power law with pegged normalization (see the XSPEC reference; Arnaud 1996).

facts imply that the X-ray pulsed emission has a magnetospheric non-thermal origin.

The observed flux indicates an (isotropic) X-ray luminosity of $L_x = 4\pi D^2 f \approx (5.7 \pm 1.0) \times 10^{32} (D/3.6 \text{ kpc})^2 \text{ erg s}^{-1}$, which corresponds to 5×10^{-4} of the spin-down power of the pulsar. The distance estimate of 3.6 kpc is based on the dispersion measure (Taylor & Cordes 1993) and is near the lower bound on the distance obtained by annual parallax (Kaspi, Taylor & Ryba 1994). If the power law spectrum extends to higher energies with a similar photon index ~ 1 , the X-ray luminosity would become as large as the spin-down power at about a few MeV. Therefore, there must be a turn off below a few MeV, consistent with the EGRET upper bound (Fierro et al. 1995).

6. Summary and Discussion

Our detection of pulsed emission in the 1.7–6.5 keV band from PSR 1937+21 reveals that the pulse is very narrow with a width of $\sim 100 \mu\text{s}$ (~ 0.06 in phase), indicating a non-thermal magnetospheric origin. There is an enhancement indicating a secondary peak, but its statistical significance is too low to be conclusive. Due to this uncertainty, we can only estimate the pulsed fraction, placing it at $\sim 40 - 60 \%$. The pulse alignment shows, within the timing errors, that the X-ray pulse is coincident with the radio interpulse. The 2–10 keV band flux (pulse + DC component) is $f = (3.7 \pm 0.6) \times 10^{-13} \text{ erg s}^{-1} \text{ cm}^{-2}$, which implies an isotropic luminosity of $L_x = 4\pi D^2 f \sim (5.7 \pm 1.0) \times 10^{32} (D/3.6 \text{ kpc})^2 \text{ erg s}^{-1}$, where D is the distance. The X-ray efficiency is $\sim 5 \times 10^{-4}$ of the spin-down power of the pulsar.

Based on ROSAT observation of the rotation powered pulsars, Becker and Trümper (1997) examined the correlation between the 0.1–2.4 keV band luminosity and the spin-down power \dot{E} . They showed that regardless the pulsar population, i.e., ordinary or millisecond pulsars, the X-ray luminosity follows an empirical law of $L_x(0.1 - 2.4 \text{ keV}) = 10^{-3} \dot{E}$.

Saito (1997) searched ASCA data for a similar correlation in the 2–10 keV band. In Figure 5, we re-examine the L_x - \dot{E} correlation in the 2–10 keV band, adding the results of this study and recent observation of PSR J2124–3358 (Sakurai et al. 1999). It is confirmed that the correlation is common to both populations and follows $L_x(2 - 10 \text{ keV}) \propto \dot{E}^{1.5}$.

As was suggested by Saito (1997), the slope in the 2–10 keV band is about 3/2 and is different from the slope of about one in the ROSAT band; the spin-down effect appears in different ways for different energy bands. Furthermore, this energy-dependent effect seems common to both populations.

In spite of a naive expectation that different magnetospheric parameters in the two pulsar populations will result in a difference in the X-ray radiation, it is difficult to discriminate between the two populations based on the L_x - \dot{E} plane.

A distinction between the millisecond pulsars and the ordinary pulsars may be found in the

pulsed emission. Among pulsars with spin-down power ranging $10^{35} - 10^{37} \text{ erg s}^{-1}$, the six data points in Figure 5 for the *ordinary pulsars* are all attributed to unpulsed emission, while the three millisecond pulsars (PSR 1937+21, PSR 1821–24 and PSR J0218+4232) in the same range of spin-down power show pulse-dominated emission. For the ordinary pulsars in Figure 5, the Crab-like pulse-dominated pulsars are only found for spin-down power larger than $\sim 10^{37} \text{ erg s}^{-1}$, and the pulsars in the range $\dot{E} \sim 10^{35} - 10^{37} \text{ erg s}^{-1}$ are Vela-like, i.e., the emission is dominated by a DC component, and only upper limits of the pulsed fraction are given, except for the Vela pulsar itself. RXTE observations of the Vela pulsar give a pulsed luminosity of $\sim 5 \times 10^{30} \text{ erg s}^{-1}$ (Strickman, Harding & de Jager 1999), which is three orders of magnitude smaller than the total X-ray luminosity of $1.2 \times 10^{33} \text{ erg s}^{-1}$ (Saito 1997) plotted in Figure 5. On the other hand, PSR 1937+21, PSR 1821–24 and PSR J0218+4232 are in the range $\dot{E} \sim 10^{35} - 10^{37} \text{ erg s}^{-1}$, but their emission is dominated by the non-thermal pulsed emission. If the *pulsed* luminosity can be measured for some of the ordinary pulsars in the range $\dot{E} \sim 10^{35} - 10^{37} \text{ erg s}^{-1}$, then we may find that the two populations can be distinguished by their location in the plane of *pulsed luminosity* versus rotation power.

Eight millisecond pulsars with still smaller spin-down power, $\dot{E} \lesssim 10^{35} \text{ erg s}^{-1}$, have been detected with ROSAT (for PSR J0030+0451, Becker et al. 2000; for others, Becker & Trümper 1999). Two of them, PSR J0437–4715 and PSR J2124–3358, are also detected with ASCA (Kawai, Tamura & Saito 1998, Sakurai et al. 1999). Pulsation is detected for three pulsars: PSR J0437–4715 shows a sinusoidal shape and a pulsed fraction of about 30%; PSR J2124–3358 shows a double-peaked profile and a pulsed fraction of $\sim 33\%$; PSR J0030+0451 also shows a double-peaked profile and a pulsed fraction of $\sim 69\%$. The X-ray and radio profiles are similar to each other for the latter two, but profile alignment has not yet been done. For ordinary pulsars with $\dot{E} \lesssim 10^{35} \text{ erg s}^{-1}$, the radiation is a mixture of several components including radiation from the cooling neutron star, the heated polar caps, the nebula and the magnetosphere. Decomposition of these components is not complete at present, and it is still difficult to compare the two pulsar populations for $\dot{E} \lesssim 10^{35} \text{ erg s}^{-1}$. Future and on-going missions should provide fruitful data to resolve the problem.

A twin of PSR 1937+21 is PSR 1821–24, which has a similar rotation power and light cylinder field as PSR 1937+21 (see Table 2). This pulsar also shows non-thermal narrow pulses with a double peaked profile in X-rays (Saito et al. 1997, Rots et al. 1998). Pulse alignment for this pulsar shows that the X-ray primary peak is nearly coincident with the radio primary pulse. It is known that pulse alignment is exceptionally good for the Crab pulsar, but is in general complicated for other ordinary pulsars, (e.g., Strickman, Harding & de Jager 1999 for the Vela pulsar; Rots et al. 1998 for PSR B1509-58; for other pulsars see references therein). It is interesting to note that the common feature among these two millisecond pulsars and the Crab pulsar is the light cylinder field strength of $\sim 10^6 \text{ G}$ (Table 2). PSR 1937+21 shares another property, giant radio pulses, with the Crab. Giant pulses of PSR 1937+21 are delayed by some 40–50 μs from the main and interpulses (Cognard et al. 1996), so are different in phase from the X-ray pulses.

Another pulsar with high light-cylinder field ($B_L = 3.2 \times 10^5$ G) and with high spin-down power ($\dot{E} = 2.5 \times 10^{35}$ erg s $^{-1}$) is PSR J0218+4232, which shows non-thermal double peaked emission (Kuiper et al. 1998, Mineo et al. 2000). X-ray pulse alignment was not possible for this pulsar given the uncertainties in absolute time of the ROSAT and BeppoSAX clocks.

The Crab-like features seen in the millisecond pulsars with large light-cylinder fields may suggest that the X-ray and radio emission originates near the light cylinder. However, the polar cap model can also account for the X-ray emission from the millisecond pulsar (Luo, Shibata & Melrose 2000). Theoretical assessment of this issue is strongly suggested.

Acknowledgments. We are deeply indebted to K. Hashimoto for his help in the spatial analysis, to K. Ebisawa (GSFC) for valuable discussions about the timing analysis, and to S. Kasahara for preparing figures for the X-ray images. The Arecibo Observatory is part of the National Astronomy and Ionosphere Center, which is operated by Cornell University under a cooperative agreement with the National Science Foundation.

This work is supported in part by a Grant-in-Aid for Scientific Research (10117203, 12640229) from the Ministry of Education, Science, and Culture in Japan.

REFERENCES

- Arnaud, K.A. 1996, in “Astronomical Data Analysis Software and Systems V”, eds. Jacoby G. and Barnes J., p17, ASP Conf. Series volume 101
- Backer, D. C., Kulkarni, S. R., Heiles, C., Davis, M. M., & Goss, W. M. 1982, *Nature*, 300, 615
- Becker, W., & Trümper, J. 1997, *A&A*, 326, 682
- Becker, W., & Trümper J. 1999, *A&A*, 341, 803
- Becker, W., Trümper, J., Lommen, A. N., & Backer, D. C. 2000, *ApJ*, 545, 1015
- Buccheri R., et al. 1983, *A&A*, 128, 245
- Burke, B.E., et al. 1991, *IEEE Trans.*, ED-38, 1069
- Burke, B.E., et al. 1994, *IEEE Trans. Nuclear Science*, 41, 375
- Cognard, I., Shrauner, J. A., Taylor, J. H., & Thorsett, S. E. 1996, *ApJ*, 457, L81
- Fierro, J. M., et al. 1995, *ApJ*, 447, 807
- Gotthelf, E. 1996, *ASCA News*, No.4, 31
- Kaspi, V. M., Taylor, J. H., & Ryba, M. F. 1994, *ApJ*, 428, 713

- Kawai, N., Tamura, K., & Saito, Y. 1998, *Adv. Space Res.*, Vol 21, NO 1/2, 213
- Kramer, M., Lange, C., Lorimer, D. R., Backer, D. C., Xilouris, K. M., Jessner, A., & Wielebinski, R. 1999, *ApJ*, 526, 957
- Kuiper, L., Hermsen, W., Verbunt, F., & Belloni, T. 1998, *A&A*, 336, 545
- Luo Q., Shibata, S., & Melrose, D. B. 2000, *MNRAS*, 318, 943
- Makishima, K., et al. 1996, *PASJ*, 48, 171
- Mineo, T., et al. 2000, *A&A*, 355, 1053
- Ohashi, T., et al. 1996, *PASJ*, 48, 157
- Rots, A. H., et al. 1998, *ApJ*, 501, 749
- Pivovarov, M. J., Kaspi, V. M., Gotthelf, E. V. 2000, *ApJ*, 528, 436
- Saito, Y. 1997, Ph.D. thesis, University of Tokyo
- Saito, Y., Kawai, N., Kamae, T., Shibata, S., Dotani, T., & Kulkarni, S.R. 1997, *ApJL*, 477, L37
- Sakurai, I., Kawai, N., Negoro, H., Saito, Y., Torii, K., & Shibata, S. 1999, *Astronomische Nachrichten*, 320 339
- Strickman, M. S., Harding, A. K., & De Jager, O. C. 1999, *ApJ*, 524, 373
- Tanaka, Y., Inoue, H., & Holt, S. S. 1994, *PASJ*, 46, L37
- Taylor, J. H., & Cordes, J. M. 1993, *ApJ*, 411, 674
- Verbunt, F., Kuiper, L., Belloni, T., Johnston, H. M., De Bruyn, A. G., Hermsen, W., & Van der Klis, M. 1996, *A&A*, 311, L9

Table 1: Radio Ephemeris

PSR name	1937+21
R.A.(J2000.0)	19 39 38.560
Decl.(J2000.0)	21 34 59.14
MJD validity interval	50710 – 50775
$t_{0,geo}$	50742.000000003
ν_0	641.9282504747918
$\dot{\nu}_0$	-4.33167×10^{-14}
$\ddot{\nu}_0$	0.00

Note — The JPL DE200 solar system ephemeris file has been used. The value of $t_{0,geo}$ is the infinite-frequency geocentric UTC arrival time of the radio pulse (MJD), and the integer part of $t_{0,geo}$ is the barycentric (TDB) epoch of the pulsar position, pulse frequency and its time derivatives. The ephemeris contains local values of the spin frequency and dispersion measure; the other parameters were held fixed at the values given in Kaspi et al. (1994).

Table 2: Parameters of the millisecond pulsars with large rotation power and the Crab pulsar

PSR name	P (10^{-3} s)	\dot{P} (s s^{-1})	\dot{E} (erg s^{-1})	B_s (G)	B_L (G)
PSR B1937+21	1.56	1.05×10^{-20}	1.1×10^{36}	8.2×10^8	1.0×10^6
PSR B1821–24	3.05	1.62×10^{-18}	2.2×10^{36}	4.5×10^9	7.3×10^5
PSR J0218+4232	2.32	8.0×10^{-20}	2.5×10^{35}	8.7×10^8	3.2×10^5
Crab	33.1	4.22×10^{-13}	4.6×10^{38}	7.5×10^{12}	0.9×10^6

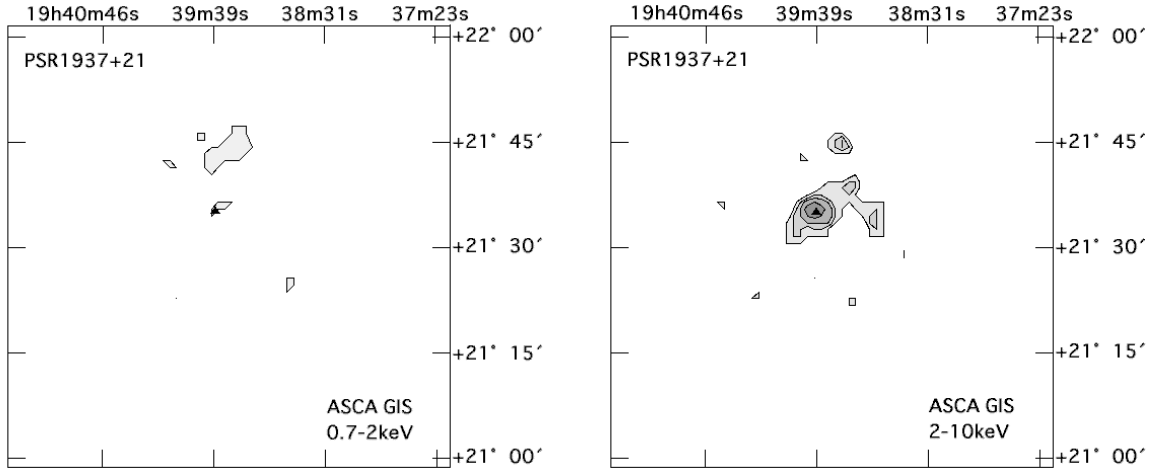


Fig. 1.— X-ray contour maps of PSR B1937+21 obtained with GIS in the 0.7–2 keV band (*left*) and in the 2–10 keV band (*right*). The contour for the soft band (*left*) is 5 counts per pixel, corresponding to 4.1σ , and the contours for the hard band (*right*) are 8, 9, 10 and 12 counts per pixel, corresponding to 3.0σ , 5.1σ , 7.2σ and 13σ , respectively. The filled triangles in the contour maps indicate the radio position of the pulsar.

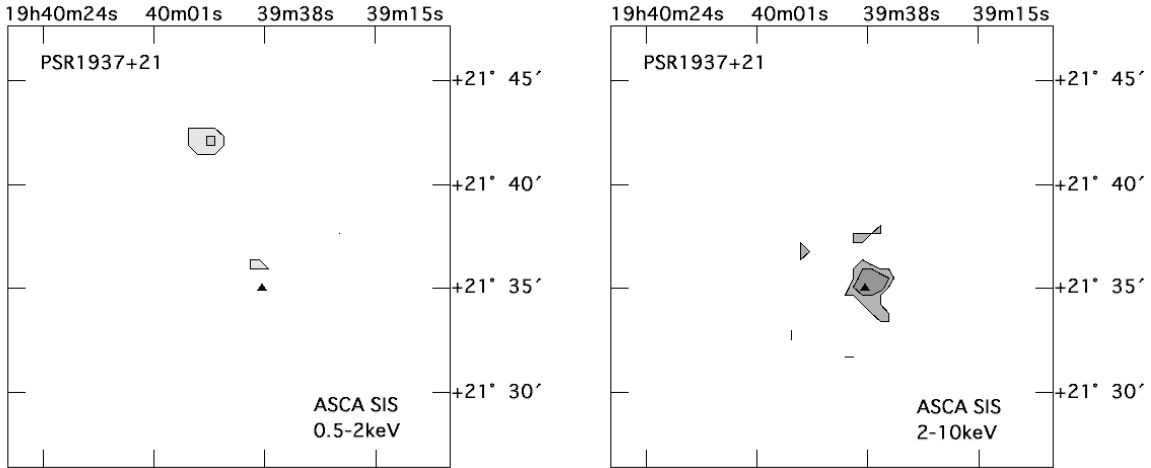


Fig. 2.— X-ray contour map of PSR B1937+21 obtained with SIS in the 0.5–2 keV band (*left*) and in the 2–10 keV band (*right*). The contours for the soft band (*left*) are 2 and 3 counts per pixel, corresponding to 4.5σ , and 10σ , respectively, and the contours for the hard band (*right*) are 3 and 4 counts per pixel, corresponding to 5.2σ and 9.9σ , respectively. The filled triangles in the contour maps indicate the radio position of the pulsar.

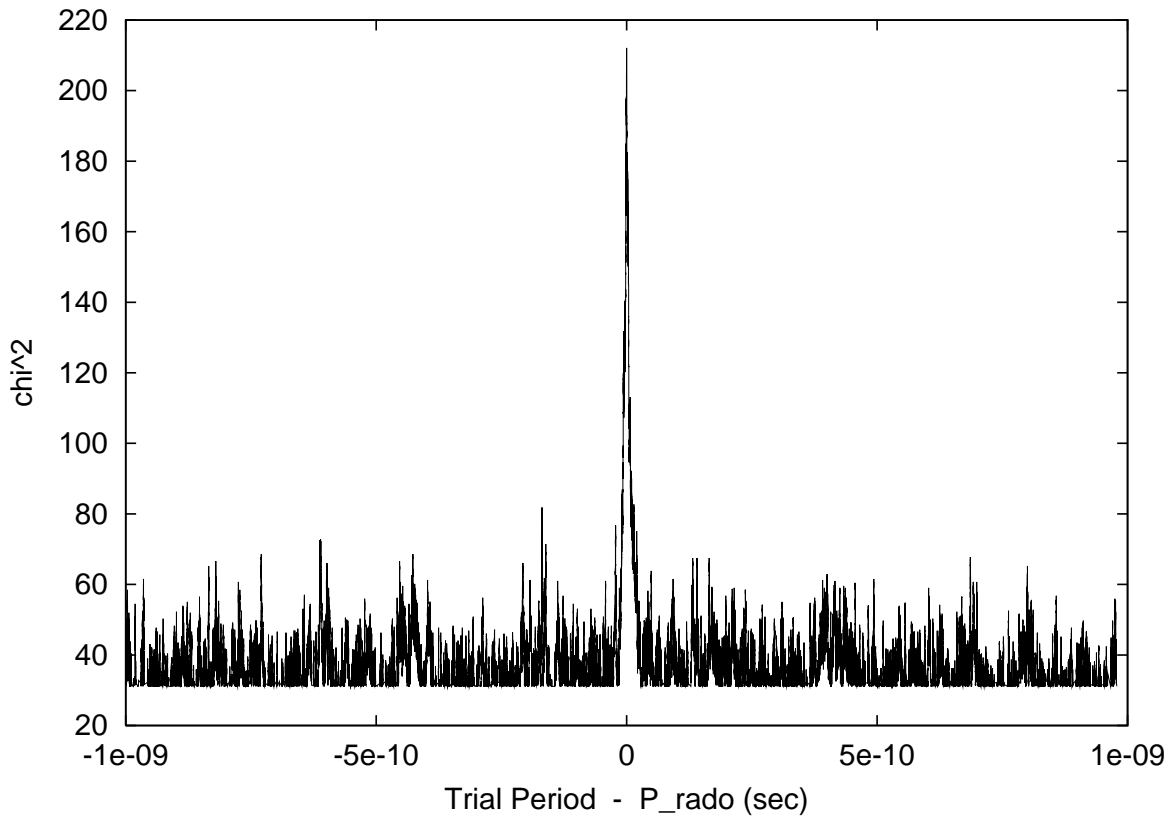


Fig. 3.— The χ^2 significances are plotted as a function of trial period. The zero point corresponds to the expected period derived from the radio ephemeris (Table 1)

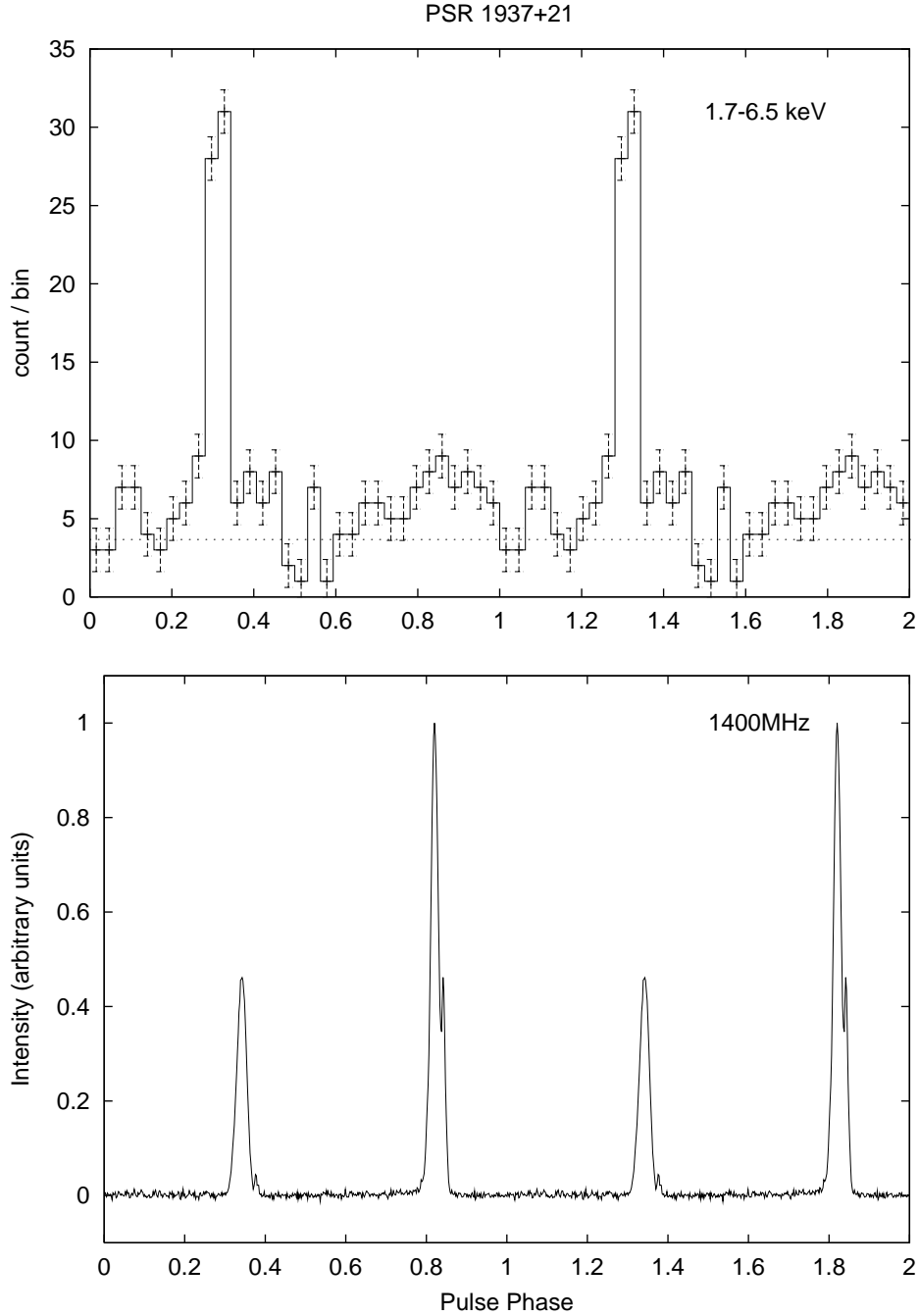


Fig. 4.— *Upper panel:* Pulse profile of PSR B1937+21 in the GIS 1.7 - 6.5 keV band. Two phase cycles are shown for clarity. The dashed line indicates the background level, 3.67 counts/bin, for a division in 32 phase bins. The bin size corresponds to $\sim 49\mu\text{s}$. *Lower panel:* The radio pulse profile at 1.4 GHz. We find that the X-ray pulse is coincident with the radio interpulse. The timing error for the alignment is about $15\mu\text{s}$ in the radio data and $100\mu\text{s}$ (0.064 phase) in the X-ray data: the timing error is roughly two phase bins in the upper panel.

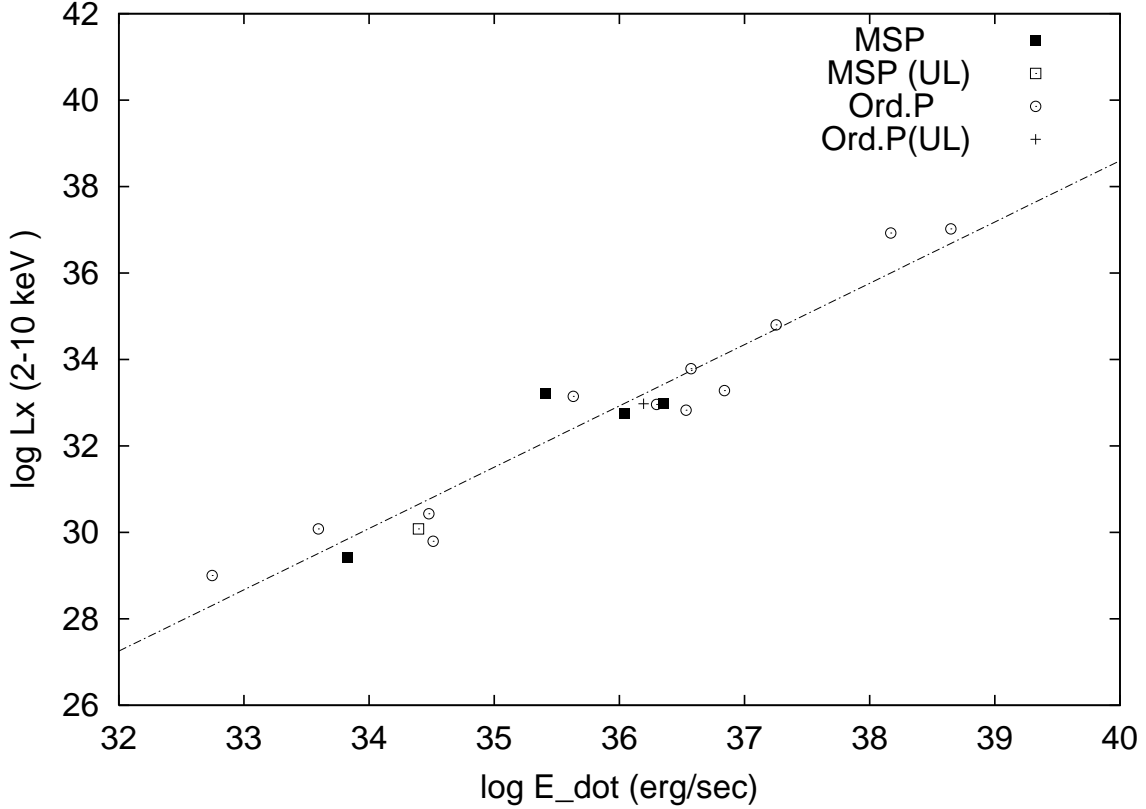


Fig. 5.— Pulsar luminosity in the 2–10 keV band versus the rotation power of the pulsars. The data are taken from Sakurai et al. (1999) for PSR J2124–3358, Pivovarov, Kaspi & Gotthelf (2000) for PSR B1046–58 and PSR B1610–50, Mineo et al. (2000) for PSR J0218+4232, Saito (1997) for others, and the present work for PSR 1937+21. The filled boxes indicate millisecond pulsars, while the open box indicates an upper limit (PSR J0437–4715). The open circles indicate ordinary pulsars, and the cross indicates an upper limit (PSR B1610–50). The regression line is given by $\log L_x = 1.45(\pm 0.09) \log \dot{E} - 19.5(\pm 3.3)$, where we used the statistical package ASURV, which is developed for the analysis of censored data (<ftp://www.astro.psu.edu/users/edf/asurv.shar>).